COBEM 2021 26th International Congress of Mechanical Engineering
November 22-26, 2021, Virtual Congress, Brazil
ABCM Associação Brasileira de Engenharia e Ciências Mecânicas

COB-2021-0604
Characterization of Vapor Compression Refrigeration Cycles through the Second Law of Thermodynamics

Vinicius Akyo Matsuda
Luben Cabezas-Gómez
Álvaro Roberto Gardenghi
Heat Transfer Research Group, Department of Mechanical Engineering, São Carlos School of Enginnering, University of São Paulo, Trabalhador São-carlense Avenue, 400, 13566-970, São Carlos, SP, Brazil
viniciusmatsuda@usp.br
lubencg@sc.usp.br
alvaro.gardenghi@alumni.usp.br

Abstract. *In this work a transient behavior of a dual-skin chest freezer refrigeration system, operating with R290, is studied numerically with the purpose of characterizing the system through the Second Law of Thermodynamics. For this aim a mathematical model which accounts for mass distribution inside the system is used. More specifically this work addresses the calculation of entropy generation and exergy destruction for characterizing the system behavior in the on-off operation. The second Law system efficiency is also estimated. In order to validate the model a comparison with measured experimental data is performed. The characterization of the system through the second law of Thermodynamics is conducted using two different methods. One consists in a direct calculation of the entropy generation rate and the other in the calculation of exergy destruction rate. The equivalence of these two methods is used as an indicative of the "correctness" of the performed calculations. The obtained results are well behaved in relation to the experimental data. The system's characterization with the second law results indicates the behavior of entropy generation, exergy destruction and second law efficiency with time in the whole system and in its components. The results are useful for improving the refrigeration system design.*

Keywords: *Transient numerical simulation, Second Law of Thermodynamics, Vapor Compression Cycle, Efficiency, R290.*

1. INTRODUCTION

Since it's creation, refrigeration systems became indispensable to the human needs, being it's use domestic or industrial, representing roughly 17% of the global energetic consumption, with about 45% of this quantity being due to the domestic use alone (IIR, 2015). In Brazil these systems were responsible for about 26.44% of the domestic electric consumption in the year of 2019 (25.72% being for refrigerator alone and 26% 0.72% for freezers) (PROCEL, 2019). These facts indicate that the optimization of the energetic consumption of these systems became an engineering requirement.

One way to do such optimization is through the use of second law of thermodynamics. This may include the analysis of the relation of the system COP (coefficient of performance) and the maximum COP achievable for the same system, i.e., the second law efficiency). Also this can be performed by the computation of the thermodynamic irreversibilities that occur during the system operation regimes. The realization of these calculation needs a robust model that can simulate the system transient and stead-steady regimes and allow the application of entropy and exergy balances to characterize the system behavior.

In this article a refrigeration system of a dual-skin chest-freezer using propane (R290) as refrigerant is studied numerically, addressing the system's transient behavior and performance. The main aim of the study is to perform a system's second law analysis when performing pull-down and on-off operations. For this purpose the capacitive model presented by (GARDENGHI, 2020; Gardenghi *et al.*, 2021) was modified to enable the second law calculation. After that the data provided by the authors where used to validate the changes made in the model.

Accordingly to the literature review, one previous model that addressed the second law aspects of the refrigeration system operation was done using a lumped parameter model (Yang and Ordonez, 2018), much alike the one presented in this work. Other work used lumped parameter moving boundaries model (Jain and Alleyne, 2014). Both works focused mainly on the *pull-down* operating regime. These two models make use of the numerical integration approach for the system very similar to that developed in the present work.

The paper is organized as follows. Methodology, including the modifications made in the model presented by GARDENGHI (2020), and the derivation of the transient exergy destruction rates and the entropy generation rates a in Vapor Compression Cycles (VCC), are provided in Section 2. Simulation results using the modified model, a comparison with

experimental data and the results regarding the second law of thermodynamics are presented in Section 3. In this sections it is also provided the results discussions. Finally the conclusions of the paper are presented in Section 4.

2. METHODOLOGY

2.1 Mathematical Model

The models employed in this paper are those developed by GARDENGHI (2020); Gardenghi *et al.* (2021) and based on Jakobsen (1995), with the necessary modification to perform the Second Law Analysis of the system and its components. In summary, the model used is composed by "sub-models" for each main component (compressor, condenser, capillary tube, evaporator and cabinet compartment), were each "sub-model" is a set of ordinary differential algebraic equations (DAEs) that are solved numerically to perform the simulation of the system along it's operation time. These equations are mainly the mass conservation and the energy conservation balances, that allow the computation of parameters such as the contains of refrigerant in the main components and the estimation of the degrees of sub-cooling and super-heating, as well as component temperatures and pressures. The control volumes adopted and the interaction between components are shown in Fig. 1.

To enable the implementation of the model are considered the same simplifying hypothesis originally adopted by GARDENGHI (2020); Gardenghi *et al.* (2021). These are: ***(i)*** control volumes of the system components have only one inlet and one outlet; ***(ii)*** kinetic and potential energies within and at the open boundaries are neglected; ***(iii)*** the thermodynamic and transport properties are uniform in each control volume; ***(iv)*** force fields are neglected; ***(v)***delays in transport, pressure losses and accumulation of refrigerant in the connecting tubes; pressure losses in the condenser and evaporator; spatial temperature variations on the surfaces of the condenser, evaporator and compressor and within the cabinet compartments are all neglected. The simulations do not consider the opening of doors, following the conditions of the experimental tests. Air infiltration is not taken into account. Only the main changes performed in the model for calculating entropy and exergy balances will be discussed. A more detailed description of the model can be found in GARDENGHI (2020); Gardenghi *et al.* (2021).

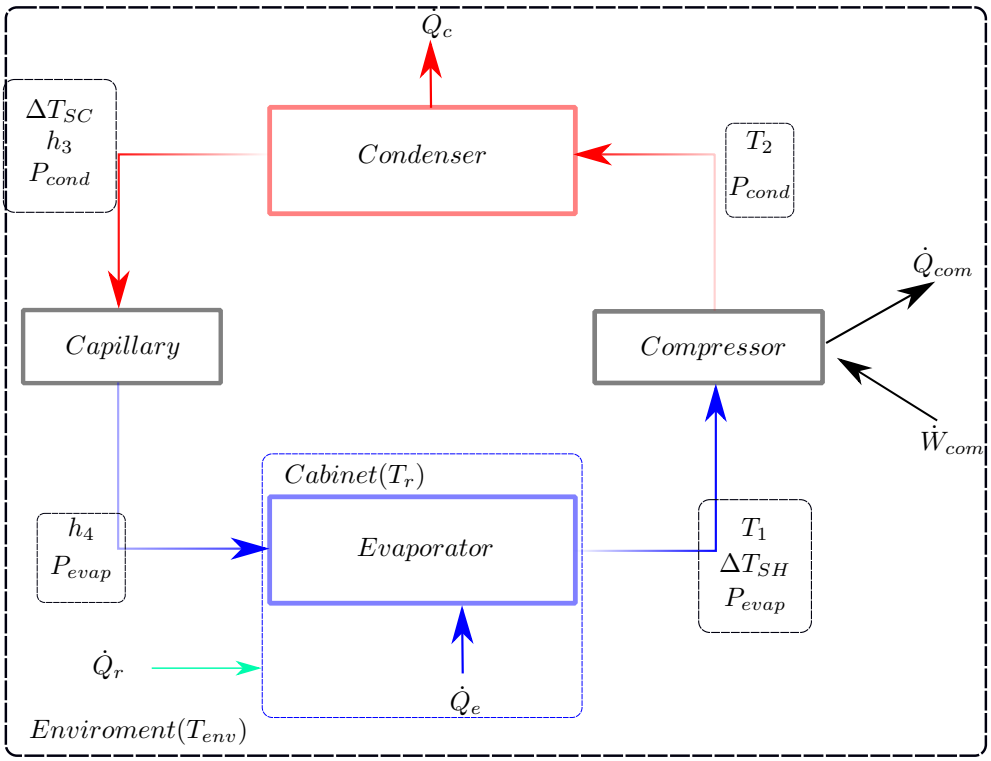

Figure 1. Control volumes and the interaction between the components

In the compressor sub-model the main change made is relative to the mass flow through the compressor when the system is turned off. For this calculation the method proposed by Ndiaye and Bernier (2010) was used. The respective method consists in the iterative calculation described bellow, its also important to note that this model assumes that any refrigerant entering into the compressor will first mix with the refrigerant already present in the shell before entering in the cylinder, and also that this mixture is thermally homogeneous. Finally, the effects of suction and discharge mufflers on the heat exchange and pressure drop are not accounted for.

1. Calculate the enthalpy of the refrigerant in the shell:

$$h_{shell} = \frac{\dot{m}_{suc} \cdot h_1 + V_{shell}\frac{dP_{evap}}{dt} + \frac{\rho^{\circ}_{shell} \cdot h^{\circ}_{shell}}{\Delta t} \forbar V_{shell}}{\frac{\rho_{shell}}{\Delta t} V_{shell}} \quad [J/kg] \tag{1}$$

2. Calculate temperature and density of the refrigerant in the shell using the suction pressure and the enthalpy of the refrigerant in the shell.

3. Using the mass conservation law, the mass flow at the compressor suction can be written as:

$$\dot{m}_{suc} = \forbar V_{shell} \cdot \frac{\rho_{shell} - \rho^{\circ}_{shell}}{\Delta t} \quad [kg/s] \tag{2}$$

4. This process must be repeated until a convergence for the mass flow and the enthalpy is reached.

In the calculations shown above, $\dot{m}_{suc}$ stands for the mass flow rate at the suction line of the compressor, h_1 is the compressor inlet specific enthalpy, h_{shell} is the specific enthalpy of the refrigerant stored in the compressor suction section (muffler and suction chamber), $\forbar V_{shell}$ is the suction section volume, ρ_{shell} stands for the density of the refrigerant stored in the compressor suction section and P_{evap} is the evaporation pressure. h_{shell} differs from h_1 due to the mixing process that occurs in the compressor shell between the refrigerant already stored in the suction section and the one that is entering into the compressor through the inlet tube.

Finally the compressor mass flow rate at the discharge line($\dot{m}_{com}$), can be estimated by assuming that the refrigerant stored in the discharge line is at equilibrium with the shell, and so the mass stored is given by:

$$M_{dis} = \rho_{dis} \cdot \forbar V_{dis} \quad [kg] \tag{3}$$

The derivative of Eq. (3) with respect to time gives the mass flow rate at the compressor discharge line and can be computed when the system is in the "off period", where $\forbar V_{dis}$ is the compressor discharge line volume.

$$\dot{m_{cap}} = a \cdot \sqrt{\frac{P_{cond} - P_{cap_{out}}}{v_3}} + b \cdot \Delta T_{SC} + c \quad [kg/s] \tag{4}$$

The mass flow rate of the capillary tube can be modeled following the Eq.(4), according to GARDENGHI (2020). The coefficients a, b and c were determined through experimental results and adjusted as: a = 0.0050416, b = 0.3460787, and c = 0. At the outlet of the capillary tube, a critical flow is possible due to the high acceleration of the fluid in the device. Thus, the Fauske (Fauske, 1962; Guzella *et al.*, 2016) criterion was implemented to determine the critical pressure, P_{crit}. The effective pressure at the outlet of the tube is calculated as $P_{cap_{out}} = max(P_{evap}, Pcrit)$.

For the both heat exchangers, changes were made in the calculation of partial derivatives relative to the parameter f_1 and f_2 defined in GARDENGHI (2020), where they were calculated in a explicit way using small time steps. Here a method more similar to the one adopted by Jakobsen (1995) for R134a was adopted, the equations for the partial derivatives are shown in Tab. 1 and their coefficients are shown in Tab. 2.

Table 1. Partial Derivatives.

f_1 Partial Derivative	$\frac{df_1}{dP} = 3\beta_1 P^2 + 2\beta_2 P + \beta_3$	(5)
f_2 Partial Derivative	$\frac{df_2}{dP} = \frac{\beta_4}{P} + \frac{\beta_5}{2} P^{-1/2}$	(6)

When the compressor is turned off, the mass flow rate through the capillary ($\dot{m}_{cap}$) will become greater than the mass flow rate in the compressor discharge, leading to a quickly pressure drop on the condenser. It is in this situation that the system will experience a temperature drop due the flash effect that will take place. Due to the complexity of this phenomenon it is hard to correctly model it in a lumped parameter model. In order to capture this phenomenon the heat absorbed by the flashing refrigerant was modeled as an external "*cold reservoir*". The heat transfer areas for the super-heated vapor (A_{sh}) and the flashing fluid (A_{flash}) were calculated by assuming a linear variation of these areas with the mass stored inside the system in super-heated form ($\dot{m}_{sh}$) and mass that must undergo the flashing process ($\dot{m}_{flash}$), as shown in Fig. 2.

Table 2. Partial Derivatives Coefficients

Coefficients	
β_1	$1.23309 \cdot 10^{-13}$
β_2	$-8.30757 \cdot 10^{-7}$
β_3	6.89189
β_4	34721.6
β_5	116.016

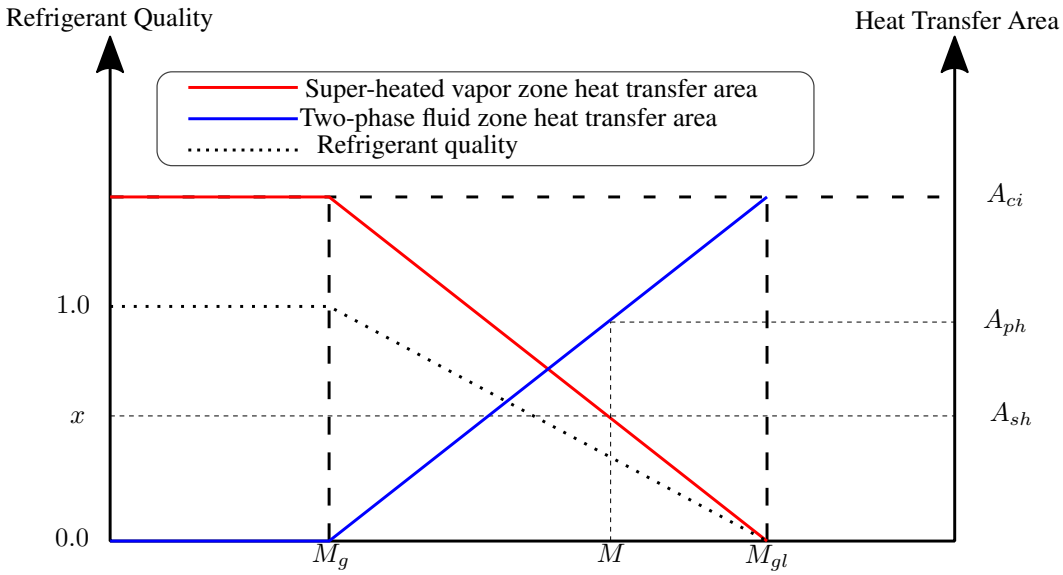

Figure 2. Approximation for the heat transfer areas inside the condenser.

In the first moments the condensing temperature will still be above the condenser wall temperature, and so, the model developed by GARDENGHI (2020) can handle it. When the condenser wall temperature becomes lower than the condenser wall temperature (T_{wc}) it is assumed that the region of the condenser occupied by the refrigerant in the two-phase state will undergo the flashing phenomenon, absorbing heat from the condenser wall. And by doing so it will cool it down, this quantity is denoted by $\dot{Q}_{flash}$ and is calculated through Eq. (8). It is easy to note that the equation is similar to Eq. (7), with respect to the the heat transfer area A_{flash}, that is calculated through Eq. (10). Another change performed in Eq. (7), is relative to bulk temperature of the refrigerant and the heat transfer area, in the new model the bulk temperature is computed by the average between the inlet an outlet temperatures in the condenser,the heat transfer area is given by Eq. (9), finally the last modification made to the model is done in order to include the Flashing Phenomenon Heat Flux to the temperature transient of the condenser wall, resulting Eq.(11).

Table 3. New equations for the condenser sub-mode.

Heat Exchanged with the refrigerant	$\dot{Q}_{cond} = h_{cond} \cdot A_{ci} \cdot [T_{med} - T_{wc}]$	(7)
Flashing Phenomena Heat flux	$\dot{Q}_{flash} = h_{reduction} \cdot h_{cond} \cdot A_{ci} \cdot [T_{cond} - T_{wc}]$	(8)
Super-Heated Zone Heat Transfer Area	$A_{sh} = A_{Ci} \cdot \left[\frac{M_{glc} - M_C}{M_{vlc} - M_{vc}}\right]$	(9)
Flashing Zone Heat Transfer Area	$A_{flash} = A_{Ci} \cdot \left[\frac{M_c - M_{vc}}{M_{vlc} - M_{vc}}\right]$	(10)
Condenser Temperature Transient when flash occur	$\frac{dT_{wc}}{dt} = \frac{\dot{Q}_{cond} - \dot{Q}_C - \dot{Q}_{flash}}{C_C}$	(11)

Although no modified or new equation for the evaporator are shown in this paper, other simple modifications of condenser and evaporator sub-models were made. When the system is turned off the mass flow rate in the condenser inlet is given by $\dot{m}_{com}$ and the mass flow rate on the evaporator outlet is given by $\dot{m}_{suc}$, instead of assuming a null value as done in the unmodified model. The same kind of modification was made for the compressor sub-model when the mass flow rates at the inlet and outlet are given by $\dot{m}_{suc}$ and $\dot{m}_{com}$, respectively.

2.2 Second Law Analysis

In the second law analysis of the system the following equations for the rate of exergy destruction ($\dot{X}_{des}$) and the rate of entropy generation ($\dot{S}_{gen}$) are used.

$$\dot{X}_{des_{Sys}} = \dot{X}_{des_{com}} + \dot{X}_{des_C} + \dot{X}_{des_{cap}} + \dot{X}_{des_E} \quad [W] \tag{12}$$

$$\dot{S}_{gen_{Sys}} = \dot{S}_{gen_{com}} + \dot{S}_{gen_C} + \dot{S}_{gen_{cap}} + \dot{S}_{gen_E} \quad [W/K] \tag{13}$$

Due to the equivalence of these concepts, two different paths can be taken to evaluate it. The exergy destroyed in the system can be evaluated through an exergy balance (Eq. (12)) and then used to calculate the entropy generation rate. Or the entropy generated can be evaluated through an entropy balance (Eq. (13)) and then used to calculate the exergy destroyed using the Guy-Stodola relation.

2.2.1 Compressor

For the compressor a quasi-steady model is assumed, which assume "zero" all time derivatives with respect to the refrigerant mass flow rate. The compressor's control volume use extended boundaries to the environment resulting in Eq. (14). The entropy generated in the system is calculated using the same control volume quasi-steady hypothesis, leading to Eq. (15).

In both equations, Eq. (14) and Eq. (15), the subscript *housing* refers to the "solid" part of the system, which can not be treated in a quasi-steady state. The term $\frac{dX_{com_{housing}}}{dt}$ is the total exergy change of the control volume, and can be calculated by the exergy definition (Eq. (16)), where the term relative to change of the system entropy over time can be calculated by it's definition, leading to Eq. (17).

It is also important to note that when the system is operating with the compressor on, the mass flow rate in the suction and discharge lines will be the same and equal to the mass flow through the compressor(m_{com}). This assumption can be done since the compressor mass flow rate will evolve to the steady-state regime much faster than the system as a whole.

Finally the compressor housing total internal energy change can be calculated through the first Law of Thermodynamics by Eq. (18).

Table 4. Equations for the compressor sub-model.

Compressor Exergy Destruction Rate	$\dot{X}_{des_{com}} = \dot{W} + \dot{m}_{suc} \cdot [h_1 - T_{env} s_1] - \dot{m}_{com} \cdot [h_2 - T_{env} s_2] - \frac{d}{dt} X_{com_{housing}}$	(14)
Compressor Entropy Generation Rate	$\dot{S}_{gen_{com}} = \dot{m}_{com} s_2 - \dot{m}_{suc} s_1 + \frac{\dot{Q}_{com}}{T_{env}} + \frac{d}{dt} S_{com_{housing}}$	(15)
Compressor Housing Exergy change	$\frac{d}{dt} X_{com_{housing}} = \frac{d}{dt} U_{com_{housing}} - T_{env} \cdot \frac{d}{dt} S_{com_{housing}}$	(16)
Compressor Housing Entropy Change	$\frac{d}{dt} S_{com_{housing}} = \frac{1}{T_{com}} \cdot \frac{d}{dt} U_{com_{housing}}$	(17)
Compressor Thermal Transient	$\frac{dT_{com}}{dt} = \frac{\dot{W}_{com} - \dot{Q}_{com} + \dot{m}_{suc} h_1 - \dot{m}_{com} h_2}{C_{com}}$	(18)

2.2.2 Condenser

As done in the compressor model, the control volume boundaries were expanded to the environment. By doing this the heat transfer rate $\dot{Q}$ will be relative to the heat exchanged with the environment ($\dot{Q}_C$) at the air external temperature, and the time derivatives relative to the condenser wall will need to be considered in the governing equations.

The exergy balance in the condenser gives Eq. (19) and the entropy balance is given by Eq. (20). In the equations, Eq. (19) and Eq. (20), the time derivatives refer to both the "*refrigerant*" and "*solid*" sides of the control volume. Considering the fact that internal energy and entropy are additive properties the exergy change can be calculate by it's definition (Eq. (21)). First, for the "*solid*" a calculation similar to the one performed for the compressor can be done. Using Eq. (11) for the internal energy change in the condenser results in Eq. (22), while the condenser entropy change is given by Eq. (25).

It is important to note that the term relative to the heat transfer during the flash phenomena in Eq. (22) will be zero when the system is operating with the compressor turned on.

For the "refrigerant" side, the total energy change is given in Eq. (24). The calculation of the total entropy change is more complicated, being applied the model proposed by Doty *et al.* (2012). First, the the total entropy change can be divided into different therms by applying the chain rule, as shown in Eq. (25). In Equation (25) the term s_c refers to the bulk specific entropy of the system, which in this case is calculated as a function of the condensing pressure and the bulk specific volume of the system(v_c). The second term of Eq. (25), $\frac{ds_C}{dt}$ is relative to the change of the bulk specific entropy with respect to time and can be obtained through Eq. (26). The partial derivatives were calculated using the *CoolProp* libraries. The specific enthalpy derivative was calculated by it's definition, resulting in Eq. (27).

The first therm of Eq. (27) can be calculated by applying the chain rule on $\frac{d(M_C \cdot u_C)}{dt}$, which will result in Eq. (28). The second therm can be obtained by applying the chain rule on $\frac{d(V_{C} \cdot \rho_C)}{dt}$, which will result in Eq. (29). The third term is relative to the condensing pressure derivative and is given by Eq. (32) when the refrigerant presents the two-phase state and Eq. (33) when the refrigerant presents only the super-heated gas state. The derivation of this expressions can be consulted in GARDENGHI (2020). Finally, it's also important to note that when the system is turned off the heat transfer heat for the "*flashing*" fluid must be included in equations Eq. (12) and Eq. (23), which will be rewritten into Eq. (30) and Eq. (31).

Table 5. Equations for the condenser sub-model.

Condenser Total Exergy Destruction Rate	$\dot{X}_{des_C} = \dot{m}_{com} \cdot [h_2 - T_{env} s_2] - \dot{m}_{cap} \cdot [h_3 - T_{env} s_3] - \frac{d}{dt} X_{C_T}$	(19)
Condenser Total Entropy Generation Rate	$\dot{S}_{gen_C} = \dot{m}_{cap} \cdot s_3 - \dot{m}_{com} \cdot s_2 + \frac{\dot{Q}_C}{T_{env}} + \frac{d}{dt} S_{C_{Total}}$	(20)
Condenser Total Exergy	$\frac{d}{dt} X_{V_{C_C}} = \frac{d}{dt} U_C + \frac{d}{dt} U_{C_{wall}} - T_{env} \cdot \left[\frac{d}{dt} S_C + \frac{d}{dt} S_{C_{wall}}\right]$	(21)
Condenser Wall Internal Energy	$\frac{d}{dt} U_{C_{wall}} = \dot{Q}_{cond} - \dot{Q}_C - \dot{Q}_{flash}$	(22)
Condenser Wall Entropy Change	$\frac{d}{dt} S_{C_{wall}} = \frac{1}{T_{wc}} \cdot \frac{d}{dt} U_{C_{wall}}$	(23)
Refrigerant Total Internal Energy	$\frac{dU_C}{dt} = \dot{m}_{com} \cdot h_2 - \dot{m}_{cap} \cdot h_3 - \dot{Q}_{cond}$	(24)
Condenser Entropy Change	$\frac{dS_C}{dt} = \frac{d(M_C \cdot s_C)}{dt} = s_C \cdot \frac{dM_C}{dt} + M_C \cdot \frac{ds_C}{dt}$	(25)
Condenser Specific Entropy Change	$\frac{ds_C}{dt} = \left.\frac{\partial s_C}{\partial h_C}\right\|_{P_{cond}} \cdot \frac{dh_C}{dt} + \left.\frac{\partial s_C}{\partial P_{cond}}\right\|_{h_C} \cdot \frac{dP_{cond}}{dt}$	(26)
Condenser Specific Enthalpy Change	$\frac{dh_C}{dt} = \frac{du_C}{dt} + P_{cond} \cdot \frac{dv_C}{dt} + v_C \cdot \frac{dP_{cond}}{dt}$	(27)
Condenser Specific Internal Energy Change	$\frac{du_C}{dt} = \frac{1}{M_C} \cdot \left[\frac{dU_C}{dt} - u_C \cdot \frac{dM_C}{dt}\right]$	(28)
Condenser Specific Volume Change	$\frac{dv_C}{dt} = \left[\frac{-1}{V_C} \cdot \frac{dM_C}{dt}\right] \cdot v_C^2$	(29)
Condenser Total Exergy Destruction Rate(off)	$\dot{X}_{des_C} = \dot{m}_{com} \cdot [h_2 - T_{env} s_2] - \dot{m}_{cap} \cdot [h_3 - T_{env} s_3] - \left[1 - \frac{T_{env}}{T_{cond}}\right] \cdot \dot{Q}_{flash} - \frac{d}{dt} X_{C_T}$	(30)
Condenser Total Entropy Generation Rate(off)	$\dot{S}_{gen_C} = \dot{m}_{cap} \cdot s_3 - \dot{m}_{com} \cdot s_2 + \frac{\dot{Q}_C}{T_{env}} + \frac{\dot{Q}_{flash}}{T_{cond}} + \frac{d}{dt} S_{C_T}$	(31)
Condensation Pressure	$\frac{dP_{cond}}{dt} = \frac{\frac{dU_C}{dt} - f_2 \cdot \frac{dM_C}{dt}}{V_C \cdot \frac{df_1}{dP} + M_c \cdot \frac{df_2}{dP}}$	(32)
Condensation Pressure when there is only gas	$\frac{dP_{cond}}{dt} = \frac{Z \cdot R \cdot \frac{dU_C}{dt}}{c_v \cdot V_C}$	(33)

2.2.3 Capillary Tube

A similar hypothesis to the one made for the compressor can be done for the capillary tube. And since the process that the capillary tube undergoes is assumed to be isenthalpic, the exergy destruction rate for this component is reduced

to Eq. 34. The entropy generation rate in the capillary is given by Eq. 35.

Table 6. Equations for the capillary tube sub-model.

Capillary Exergy Destruction Rate	$\dot{X}_{des_{cap}} = \dot{m}_{cap} \cdot T_{env} \cdot [s_4 - s_3]$	(34)
Capillary Entropy Generation Rate	$\dot{S}_{gen_{cap}} = \dot{m}_{cap} \cdot [s_4 - s_3]$	(35)

2.2.4 Evaporator

The model used for the Second Law analysis of the evaporator is very similar to the one used for the compressor. Thus, to avoid redundancies, the equations in Tab. 5 will be used as reference in this section for most of the equations, since the only difference will be relative to changes in the sub-index.

Again the control volume boundaries were expanded to the environment, by doing this the heat transfer rate $\dot{Q}$ will be relative to the heat exchanged with the cabinet($\dot{Q}_E$) at the air external temperature, and the time derivatives relative to the evaporator wall will need to be considered in the governing equations. In general the procedure to compute the exergy destruction and entropy generation rates in the evaporator is the same as done for the condenser, with the exception to the "flash evaporation" part, since this process does not occurs in the evaporator. Thus, in this case equations Eq. (20), Eq. (19), Eq. (25), Eq. (27), Eq. (29), Eq. (23) are used for the evaporator.

For the "refrigerant" side, the total energy change is given by Eq. (37), the evaporator wall internal energy is given by Eq. (36), the pressure change with time is presented in Eq. (39), the evaporator wall temperature transient ($\frac{dT_{we}}{dt}$) is given by Eq. (38). A more detailed description of the evaporator model used can found in GARDENGHI (2020); Gardenghi *et al.* (2021).

Table 7. Equations for the evaporator sub-model.

Evaporator Wall Internal Energy	$\frac{d}{dt}U_{E_{wall}} = \dot{Q}_E - \dot{Q}_{evap}$	(36)
Refrigerant Total Internal Energy	$\frac{dU_E}{dt} = \dot{m}_{cap} \cdot h_4 - \dot{m}_{com} \cdot h_5 - \dot{Q}_{evap}$	(37)
Evaporator Wall Temperature Transient	$\frac{dT_{we}}{dt} = \frac{\dot{Q}_E - \dot{Q}_{evap}}{C_E}$	(38)
Evaporation Pressure	$\frac{dP_{evap}}{dt} = \frac{\frac{dU_E}{dt} - f_2 \cdot \frac{dM_E}{dt}}{V_E \cdot \frac{df_1}{dP} + M_E \cdot \frac{df_2}{dP}}$	(39)

3. RESULTS

In this section, results for the on-off simulations are compared to experimental data in order to validate the modification made to the previous model. Once the model is validate the study of the system through the 2° *Law of Thermodynamics* can be done.

3.1 Comparison with experimental data

The conditions in which the test were performed are shown in Tab. 8. Since the objective here is merely to compare and validate the modifications made on the basis model, the results analysed here are only the ones relative to the condensation and evaporation pressures, and the main components temperatures. A more detailed analysis is shown in GARDENGHI (2020); Gardenghi *et al.* (2021).

Table 8. Simulation Conditions.

On-off	
Environment Temperature	$25\ ^\circ C$
Superior Temperature Limit	$-19.5\ ^\circ C$
Inferior Temperature Limit	$-22.3\ ^\circ C$
Compressor Speed	$4500\ RPM$
Refrigerant Charge	$103\ g$

Figure 3 shows the temperatures of the components variation with time, for both the simulation and the experimental

data. It is possible to notice that although the simulated condenser mean temperature does not show the abrupt change as for the experimental data, the temperature is close to the experimental one, when the condenser is about to turn on again presenting an error of $0.2161\ ^{\circ}C$. For the evaporator is possible to notice a similar behavior as the one shown in GARDENGHI (2020), which was expected, since any major changes were not made in this model.

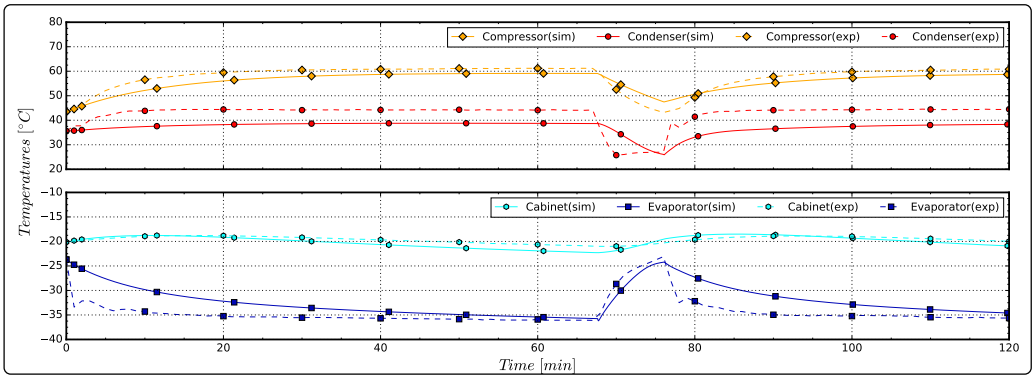

Figure 3. Components Temperatures comparison with experimental data.

The component pressures are shown in Fig. 4. It is possible to notice that both the simulated condensation and evaporation pressures show a satisfactory agreement with the experimental ones. Yet, is important to note that the simulated condensation pressure decays less abruptly than the experimental condensation pressure, which may cause a slightly different mass distribution inside the system.

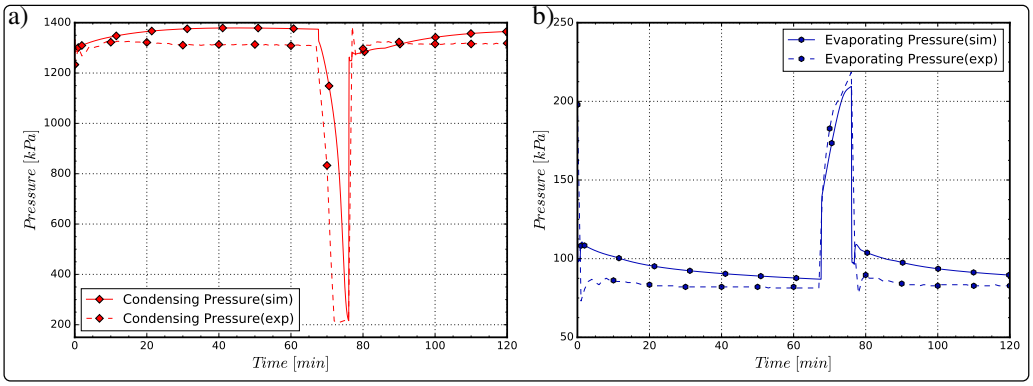

Figure 4. Components Pressures comparison with experimental data.

The modified model presented a very good agreement with the experimental data, allowing the validation of the model and in consequence the characterization of the system through the second law.

3.2 Entropy and Exergy Analysis

The conditions in which the test were performed are the ones showed in Tab. 8, Fig. 5 show the results for both the entropy generated and the exergy destroyed in the system in an on-off operating regime for a single operational cycle. It is possible to notice that during the "*on period*" the compressor will be the main cause of the system irreversibilities, followed by the capillary tube and then by the heat exchangers. When the system is turned off, both the entropy generated and the exergy destroyed by the compressor and the capillary tube will quickly go to zero. This effect is mainly due to the fact that both, the mass flow rate produced by the compressor and the mass flow rate through the capillary tube decay to zero in the first moments of the "*off period*". During this regime the condenser will be the main cause of irreversibilities in the system, this can be justified by the flash evaporation process that takes place in the condenser when the compressor is turned off.

The major term influencing the entropy generated calculated by Eq.(15) in the compressor control volume is the heat transfer from the compressor to the external environment. However these overall thermodynamic losses are due to the various internal irreversibilities taking place inside the compressor, that make this component the one with the highest entropy generation of the refrigeration system. Some processes that generate entropy inside the compressor are: heat transfer inside compression cylinder, back flow in the compressor valves and exit line, fluid friction in the compressor internal tubes and mufflers, friction between metals due to mechanical parts movement, thermal losses in the electrical motor, and others.

A more detailed graph with main terms used to calculate the entropy generated in the heat exchangers can be seen in Fig. 6. In the legend, the terms *Condenser Wall*, *Evaporator Wall* and *Refrigerant* refer to the total entropy change of these parts. For the condenser it is possible to notice that when the compressor is on the main terms of the entropy generated in the system will the heat rejected by the condenser to the external ambient and the mass flow rate throughout the system. When the compressor is turned off, the entropy contribution made by the flashing evaporation effect (here modeled as a cold source) and the one made by the condenser wall will present similar behaviors with different signals. In general the behavior of the entropy generated in the evaporator is shown to be similar to the one present by the condenser. When the compressor is operating in a "*on regime*" both the mass flow rate and the heat exchanged with the refrigerator will be the main terms of the total entropy generated in the system. But when the system is turned off the entropy generated in the system will be mostly due to the heat flow in the system, with a small contribution from the other sources.

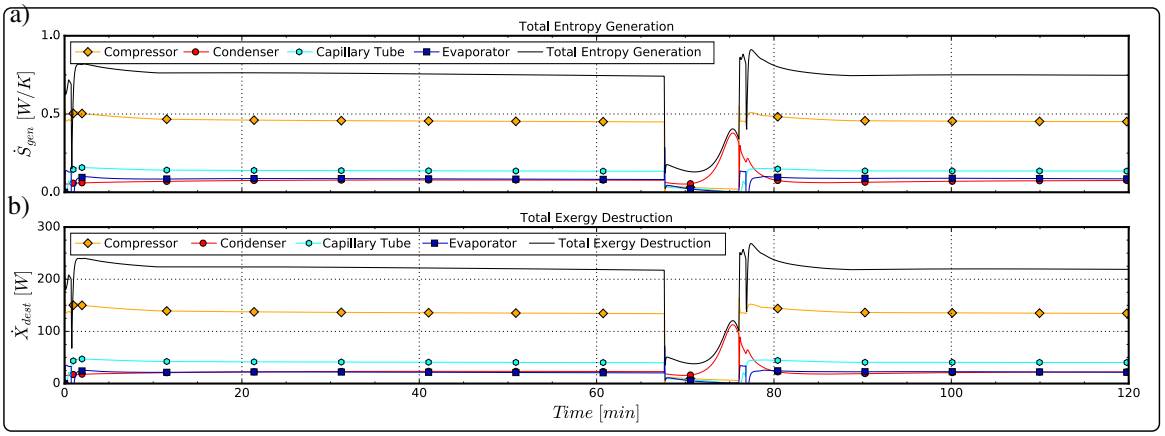

Figure 5. a) Total entropy generation rate on the system and it's main terms. b) Total exergy destruction rate on the system and it's main terms.

Finally the results regarding the *Second Law Efficiency* and the *COP*(Coefficient of Performance) are shown in Fig. 7. In this figure it is easy to note that the system operates with an efficiency close to 15% when the compressor is operating. When the system is turned off both the *COP* and the *Second Law Efficiency* were assumed to be zero, since the compressor does not operates and so it does not consumes power. The instantaneous COP shows a similar behavior as the second law efficiency. The system operates with a COP less than *1.0* when the compressor is on, having a similar behavior as the one presented by the *Second Law Efficiency*.

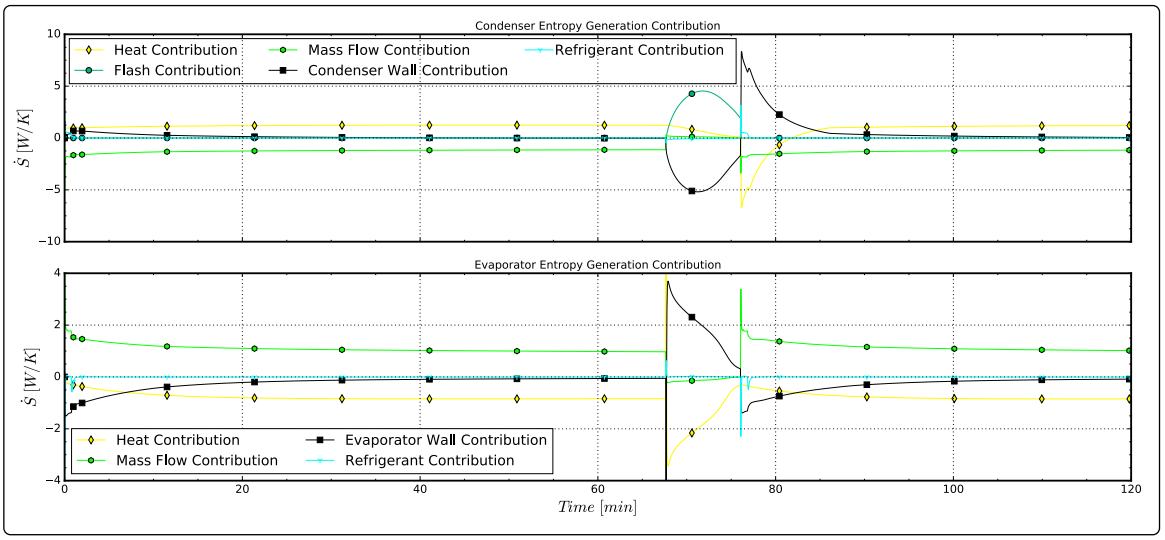

Figure 6. a) Condenser entropy generation rate contributions. b) Evaporator entropy generation rate contributions.

4. CONCLUSION

In the present work, a numerical model for computing the *Second Law of Thermodynamics* on a mechanical vapor compression domestic refrigeration system was developed. The changes made in the original model were validated by the comparison of the numerical results with the experimental data available. The second law results obtained trough the

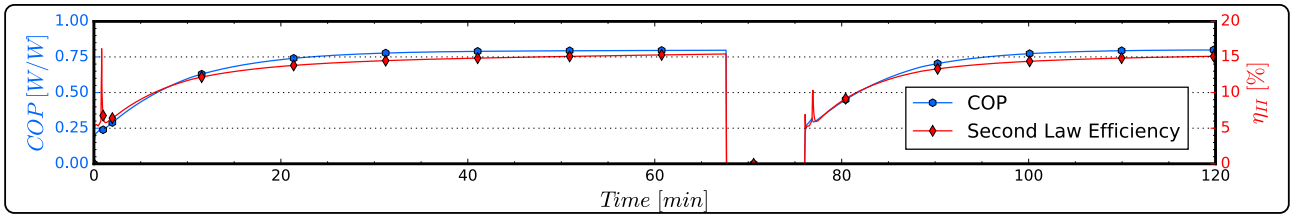

Figure 7. System instant second law efficiency and COP.

simulations were coherent with the expected ones from theory. In the paper it is presented in details what are the mains terms that produce the entropy generation in the heat exchangers.

When the system is operating in it's "on regime", the main component of the entropy generation will be the compressor, followed by the capillary tube and the heat exchangers. Then, one of the reasons for the low Second Law Efficiency(η_{II}) and COP can be associated to a over-sized compressor, causing higher system entropy generation. As the compressor delivers a cooling capacity higher than the necessary, it will turn-off and turn-on more times, operating in a more inefficient regime and affecting the system efficiency.

By analysing the results relative to the component's entropy generation rate in the system it is possible to observe the more influencing components and terms, which can be used in a more specific entropy generation minimization in the system. In these results it is also possible to notice that when the compressor is turned off the main term of the entropy generated in the whole system is the "Flashing Evaporation Phenomenon" that takes place in the condenser.

Finally it is noticed that the system operates with a relative low efficiency, showing that there is still room for improvement in system operating conditions. The increase in the system efficiency(η_{II}) can be obtained by the minimization of the entropy generated in the compressor and in the capillary tube, since both components represent the main sources of exergy destruction in the system. One solution for this problem is the use of a variable speed compressor. Future studies will be develop to address this issue.

5. ACKNOWLEDGEMENTS

The authors would like to acknowledge the support received from São Carlos School of Engineering (EESC-USP).

6. REFERENCES

Doty, J., Camberos, J. and Yerkes, K., 2012. "Approximate approach for direct calculation of unsteady entropy generation rate for engineering applications". In *50th AIAA Aerospace Sciences Meeting including the New Horizons Forum and Aerospace Exposition*. p. 1286.

Fauske, H.K., 1962. "Contribution to the theory of two-phase, one-component critical flow". doi:10.2172/4749073. URL `https://www.osti.gov/biblio/4749073`.

GARDENGHI, A.R., 2020. *Transient modeling of vapor compression refrigeration systems for domestic applications*. Masters dissertation, Mechanical Engineering Department - São Carlos School of Engineering, University of São Paulo, São Carlos, Brazil.

Gardenghi, A.R., Campanini, M.M., Lacerda, J.F., Tibiriça, C.B. and Cabezas-Gómez, L., 2021. "A detailed study of the transient behavior of a domestic vaporcompression refrigeration system with r290". *Under revision, International Journal of Refrigeration*.

Guzella, M.d.S., Cabezas Gómez, L., Guimarães, L.G.M. and Tibiriçá, C.B., 2016. "A modified approach for numerical simulation of capillary tube-suction line heat exchangers". *Applied Thermal Engineering*. doi: 10.1016/j.applthermaleng.2016.03.139.

IIR, 2015. *The role of refrigeration in the global economy*. 29th Informatory Note on Refrigeration Technologies/November 2015.

Jain, N. and Alleyne, A., 2014. "Transient exergy destruction analysis of a vapor compression system".

Jakobsen, A., 1995. "Energy optimization of refrigeration systems". *Doctoral thesis, Technical University of Denmark (DTU)*.

Ndiaye, D. and Bernier, M., 2010. "Dynamic model of a hermetic reciprocating compressor in on–off cycling operation (abbreviation: Compressor dynamic model)". *Applied Thermal Engineering*, Vol. 30, No. 8-9, pp. 792–799.

PROCEL, E., 2019. "Pesquisa de posse e hábitos de uso de equipamentos elétricos na classe residencial 2019". Available in: `https://eletrobras.com/pt/Paginas/PPH-2019.aspx`.

Yang, S. and Ordonez, J., 2018. "Integrative thermodynamic optimization of a vapor compression refrigeration system based on dynamic system responses". *Applied Thermal Engineering*, Vol. 135, pp. 493–503.